Biointerface Research in Applied Chemistry
Open-Access Journal (ISSN: 2069-5837)

Article
Volume 14, Issue 2, 2024, 28
https://doi.org/10.33263/BRIAC142.028

(Z)-2-(4-chlorophenyl)-N'-Hydroxyacetimidamide as a Human Carbonic Anhydrase Inhibitor: Synthesis, Crystal Structure, STRING Analysis, Molecular Docking and Dynamic Simulation Studies

Ramakrishna Belathur Narasaiah [1], Jayashankar Jayaprakash [2], Navya B. Suresh [2], Nanjundaswamy Shanthappa [2], Puttaswamappa Mallu [2], Shroff R Kumaraswamy [3,*]

[1] Department of Physics, Government College for Women (Autonomous), Mandya, Karnataka 571 401, India
[2] Department of Chemistry, SJCE, JSS Science and Technology University, Mysuru, Karnataka 570 006, India
[3] Department of Physics, Maharani's Science College for Women, Mysuru570 006, Karnataka, India
[*] Correspondence: kumar3130swamy@gmail.com;

Scopus Author ID 57660876900
Received: 23.01.2023; Accepted: 19.03.2023; Published: 3.02.2023

Abstract: Carbonic anhydrase (CA), an enzyme that hydrates carbon dioxide and dehydrates carbon monoxide is a promising target for developing potential anticancer agents. In the current study, a novel 2-(4-chlorophenyl)-N'-hydroxyethanimidamide (CPHA) compound is designed and tested against CA to investigate its inhibitory potential. Synthesized CPHA is characterized by various spectroscopic techniques. The molecular structure of the compound was confirmed by the single-crystal X-ray diffraction studies. The crystal structure is stabilized by O-H...N and N-H...N hydrogen bond and C-H…π stackings, which are quantified by Hirshfeld surface analysis. ADME and toxicity of the compound are analyzed, and Swiss target prediction of the compound has been carried out to analyze the preferred target. Protein-protein interaction studies have been performed to analyze the favored protein using String software. Further, a molecular docking study of CPHA compound with carbonic anhydrase protein (PDB ID:1ZNC) showed various interactions lead to a good binding score. In order to determine the stability of the interactions, molecular dynamics (MD) was calculated for 100 ns. The RMSF, RMSF, and hydrogen bonds were calculated for the 100 ns trajectory period. MD studies demonstrated that the 1ZNC-CPHA was stable during the simulation period.

Keywords: Crystal structure; MD; Carbonic anhydrase; STRING; Molecular Docking

1. Introduction

Amidoxime and its derivatives are important intermediates for synthesizing nitrogen heterocycles, particularly physiologically active oxadiazoles, in drug discovery and design. Since the amidoxime contains an amino (-NH_2) group and a hydroxyimino (=N-OH) group at the same carbon atom, it possesses the fused functionality of an amide, oxime, amidine, and a hydroxamic acid. Hence, amidoximes belong to the oximes class; they are adaptable building components that can be used to create different heterocycles. Antiglaucoma, anti-arthritic, and cardiotonic are some examples of successful medication candidates having amidoxime moiety. Amidoxime itself is often seen as a bioisostere for a carboxylic group. However, the 1,2,4-oxadiazole ring's creation is the main use of these building blocks subtype in drug design. It is an important group of heterocyclic compounds in the field of medicinal chemistry due to its

diverse biological activities, including antioxidant [1], DNA cleavage activity [2], antimalarial [3], antileishmanial agents [4], anticancer [5] and anesthetic [6] activities.

Additionally, cellulose derivatives with amidoxime functionalization are employed as a reducing and stabilizing agent in producing gold nanoparticles [7]. The functional groups within amidoxime that can engage with carbon dioxide, amine, and hydroxyl are identical, yet they exhibit marginally distinct binding modes and energies [8]. Several variations of crystal structures for amidoxime derivatives have been documented in the structural database [9-12]. In this context, we have synthesized and crystallized a novel 2-(4-chlorophenyl)-N'-hydroxyacetamidine characterized by various spectroscopic techniques. X-ray diffraction investigations further confirmed the 3D single-crystal structure. Analysis was done on the crystal packing's 3D topology, energy framework calculations, and Hirshfeld surface analysis. The HOMO-LUMO energies, their energy gap, and related characteristics were calculated using the DFT method. The Swiss Target Prediction tool was used to determine the most likely macromolecular target in order to evaluate the inhibitory potential of the title compound, where the carbonic anhydrase (CA) VII, I, III, VI, XII, XIV, XI, IV, VIII and V are predicted as the most suitable targets. CA is an enzyme that hydrates carbon dioxide (CO_2) and dehydrates carbon monoxide (HCO_3) and is a promising target for the development of potential anticancer agents [13-15]. Inhibitors of CA's have the potential to treat a number of illnesses, such as cancer, diabetes, and other metabolic syndromes. Molecular docking and dynamic simulation study was carried out to analyze the inhibitory potential of the title compound.

2. Materials and Methods

2.1. Experimental.

All solvents and reagents were purchased from Sigma Aldrich Chemicals Pvt Ltd and Merck. Reaction progress was monitored by thin-layer chromatography on silica gel GF254 aluminum sheets. The spots were detected under UV light ($\lambda = 254$ nm) chamber. The melting range was determined by the Veego melting point VMP III apparatus. Elemental data are collected by FLASH EA 1112 series of CHN analysis. 1H NMR spectra were recorded on Agilent-NMR. The UV-visible spectrum was recorded in the Shimadzu UV-1800 UV-visible spectrophotometer. The FT-IR analysis was performed using the Perkin Elmer Spectrum 1000 Instrument.

2.2. Synthesis of 2-(4-chlorophenyl)-N'-hydroxyacetamidine.

A mixture of excess sodium carbonate, parachlorobenzyl cyanide, and hydroxylamine hydrochloride was ingested and refluxed for eight hours in ethanol. The progress of the reaction was followed by TLC until the reaction was complete. After completion, the solvent was drained under light pressure. The product was saturated with chloroform and pet ether as solvents. The purified compound was obtained in good yield and crystallized using a slow evaporation technique by methanol (Scheme 1).

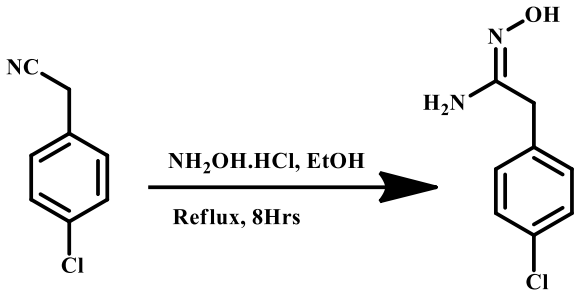

Scheme 1, Reaction pathway of 2-(4-chlorophenyl)-N'-hydroxyacetamidine.

2.3. Single crystal X-ray crystallography.

A colorless rectangle-shaped defect-free single crystal of 2-(4-chlorophenyl)-N'-hydroxyacetamidine (CPHA) was selected for data collection. X-ray intensity data were collected at a temperature of 293 K, on RigakuXtaLAB Mini X-ray diffractometer using MoKα radiation of wavelength λ= 0.71073 Å. X-ray intensity data were collected for various angular settings of φ, from 0° to 360° with a scan width of 0.5° and the sample to detector distance of 50.0 mm. A complete data set is processed using the software CRYSTAL CLEAR [16]. All the frames could be indexed by a primitive monoclinic lattice. The structure was solved by direct methods and refined by the full-matrix least-squares method on F2 using SHELX programs [17]. Positions of all the non-hydrogen atoms were revealed by the first difference Fourier map. All the hydrogen atoms were positioned geometrically (C-H = 0.93 Å, O-H = 0.82 Å). The geometrical calculations were carried out using PLATON [18]. The molecular and packing diagrams were generated using MERCURY [19].

2.4. Density functional theory calculation.

Density functional theory (DFT) is used to compute the electronic wave functions of CPHA. The preeminent approximation to the wave functions is its lowest energy state, and this can be attained by optimizing the molecular coordinates to its ground state level. The most stable calculated conformation is the basis for further theoretical calculations. CPHA molecular structure is optimized in the gas phase using DFT with B3LYP hybrid functional at 6-311G+(d,p) level basis set. The KohnSham molecular orbitals, their energy gap, and the related global and local indexes were explored with Koopman's approximation. The molecular electrostatic potential (MEP) map shows the electronegative and electropositive active sites of the molecule. All these calculations were executed using the Gaussian 16 package and were visualized using GaussView [20, 21].

2.5. Hirshfeld surfaces, Enrichment, and interaction energy calculation.

The 3D Hirshfeld surfaces (HS) and 2D fingerprint plots are unique for any crystal structure. The 2D fingerprint plots can give a quantitative summarization of the nature and type of intermolecular contacts experienced by the molecules in the crystal. At the same time, it can also be broken down to give the relative contribution to the HS area from each type of interactions present, quoted as the "contact contribution". The normalized contact distance dnorm based on de (the closest external distances from a given point on the HS), di (the closest internal distances from a given point on the HS), and the Vander Wall radii of the atom help to identify the regions of particular importance to intermolecular interactions. The combination of de and di in the form of a two-dimensional fingerprint plot summarizes intermolecular

contacts in the crystal. Visualization of the electrostatic, dispersion, and total energy components in the form of energy frameworks sheds light on the architecture of molecular crystals and, in turn, reveals the actual crystal properties. The energy framework calculations were carried out using the B3LYP/6-31G (d,p) functional basis set. A cluster of molecules within a radius of 3.8 Å and 20 Å were generated around a single molecule for interaction energy and lattice energy, respectively. The interaction energies (electrostatic, polarization, dispersion, and repulsion) between the molecular pairs and the lattice energy of the molecule were calculated using Crystal Explorer [22].

2.6. ADMET.

The standard pharmacokinetics (absorption, distribution, metabolism, excretion, and toxicity) for CPHA were determined to estimate the physicochemical and pharmacokinetics parameters in the drug discovery process [23]. The CPHA molecular structure was drawn on Marvin JS software in 2-D structure format and imported into SMILES at the website's interface (http://swissadme.ch/). The SMILES of the compound were inserted into pkCSM online tool [24]. The pkCSM online tool was used to predict ADME and toxicity, including intestinal absorption, skin permeability, BBB permeability, CNS permeability, renel OCT 2 substrate, AMES toxicity, oral rat acute toxicity, oral rat chronic toxicity, and minnow toxicity.

2.7. Swiss Target Prediction.

The first step in understanding the molecular mechanisms behind the bioactivity of small molecules is to identify their targets. The vast amount of data on protein-small molecule interactions accrued in recent years has allowed researchers to create ligand-based target prediction methods [25-28]. The SwissTargetPrediction is a free web tool for determining the targets of the potential active ingredients. This web server uses a mix of 2D and 3D similarity measurements with known ligands to predict the targets of bioactive compounds precisely [29-30]. CPHA molecule was submitted to the SWISS for target prediction. The database suggested numerous targets; the top 10 targets with probability > 0 were retrieved, and the duplicate targets were eliminated, resulting in a list of 100 targets. The discovered targets for CPHA compound were tabulated in Table 6.

2.8. Molecular docking studies.

To investigate the effect of CPHA molecule with predicted protein, molecular docking analysis was carried out using MGL tools 1.5.6 with Auto Dock vina [31, 32]. From the protein Data Bank (www.rcsb.org), a recently resolved three-dimensional X-ray crystal structure of SWISS predicted protein (PDB 1D: 1ZNC) was downloaded in PDB format. Then, using Auto Dock Tools (ADT), non-polar hydrogen atoms were added, and energy was minimized to the protein. Then the prepared structure of the receptor was saved in PDBQT format. The grid box was activated by targeting the active site with a size of (x= 40, y= 40, z= 40), and a center of (x=4.032, y=4.02 and z=14.32) was set to encircle the binding site for 1ZNC protein and the bioactive conformations was simulated [13-15]. Through the Auto dock Vina 1.5.6 tool, Virtual molecular docking and analysis have been accomplished. The ligand compound has been docked into the active sites of 1ZNC protein.

2.9. Molecular dynamic simulation studies.

The MD simulation of a 1ZNC-CPHA complex was carried out using the academic version of the Desmond modules in the Schrodinger 2020–2 suite [33]. A better docking result was chosen for the molecular dynamics (MD) simulation to determine the DMC stability with the targeted protein. The cubic box was inundated with TIP3P water molecules with a simple point charge. The system was solvated, and the OPLS3 force field was used to prepare and evaluate the complex. To keep the system neutral, the minimum quantity of Na+ ions and salt atoms was added [34]. The compound was introduced using a conjugated algorithm with a 1 Kcal/mol convergence threshold. The relaxed system was then subjected to 100ns MD simulations with a Marlyna-Tobias-Klein barostat set to 1 bar pressure and a Nose-Hoover thermostat set to 300K under NPT ensemble. The energy potential stability of the protein-ligand complex system and protein-ligand interaction were investigated using a root mean square deviation (RMSD), root mean square fluctuations (RMSF), and hydrogen bond fingerprint profile.

2.10. Protein network analysis.

Determining the total physiological impact of inhibiting a single protein requires analyzing a protein expression network [35]. The protein-protein interaction (PPI) network connected with CA protein was predicted using STRING v11.0. STRING currently contains 24.6 million proteins and over 2000 interactions from 5090 organisms and infers functional linkages utilizing three evolutionary-based prediction channels: neighborhood, fusion, and gene co-occurrence [36]. This server also predicts co-expression utilizing huge gene expression datasets and gene-by-gene correlation tests.

3. Results and Discussion

3.1. Chemistry.

The title compound is prepared by parachlorobenzyl cyanide, hydroxylamine hydrochloride, and excess sodium carbonate condensation. It is soluble in chloroform and pet ether. The elemental analysis (C, H, N) results are agreed with the calculated values. The structure of the compound is also confirmed by FT-IR, 1H-NMR, FT-IR, and UV-visible and single-crystal XRD analysis. The crystals of the compound were grown by the slow evaporation method using methanol.

3.2 Spectroscopic Characterization

Mass spectrum of 2-(4-chlorophenyl)-N’ hydroxyacetamidine was recorded on synaptic G2 HDMS Acquity UPLC spectrometer using the electron impact technique. The molecular ion peak observed at m/z = 185.12 [(M)+] is in good agreement with the calculated molecular weight of $C_8H_9ClN_2O$ 184.02. The 1H NMR spectrum of 2-(4-chlorophenyl)-N’-hydroxyacetamidineis shown in figure 1a. There is a sharp singlet at 4.48 ppm corresponding to the 2 protons of the NH_2 group and another sharp singlet at 3.41 ppm corresponding to the 2 protons of the CH_2 group. The two doublets at 7.26 and 7.19 ppm correspond to 4 protons of the aromatic phenyl ring. The proton spectral data agree with respect to the number of hydrogen and their chemical shifts with the proposed structures. The observed frequencies and their relative intensities of amidoxime, are shown in Figure 1b. In the IR spectrum, there are two

strong bands in the region 3481 and 3372 $cm^{-1,}$ which is assign to the primary amine stretching frequency. The O-H stretching of amidoxime observed a wide band at 3143 cm^{-1}. C=N stretching band occurs in the region 1690-1620cm-1 in the present case, C=N assigned to the strong band at 1655cm^{-1}. The C-H deformation vibration in CH2 is observed at 1487 cm^{-1}. The appearance of bands at 1587 and 1421 cm-1 due to the bending and stretching vibration of phenyl C=C bonds, respectively. The bands at 966 and 806 indicate the presence of aromatic bending vibration and twisting vibration, respectively. The absorption peak at 1192cm^{-1} is due to the C-N stretching vibration. C-Cl stretching vibration is at 735 cm^{-1}. The UV-visible -NIR spectrum was recorded for the grown crystal in the range 200–1200 nm using a Shimadzu UV-1800 spectrophotometer. The optical absorption and transmittance spectra of the title compound are shown in Figures 1c and 1d. The absorption spectrum reveals the crystal has strong absorption in the region 200 to 380 nm. The UV-visible spectra of the compound displayed $\pi \rightarrow \pi*$ transition of the benzene ring at 290 nm, and the band that appeared at 360 nm corresponds to $n \rightarrow \pi*$ transition of constituent functional groups (=N–OH and $–NH_2$). The UV spectra show less transparency window and maximum absorption. The visible spectra show more transparency and less absorption. The optical band gap energy of the grown crystal was calculated using the formula Eg =1240/λ (nm) in eV, where λ is the lower cut-off wavelength (385 nm). The band gap of the crystal was found to be 3.22 eV.

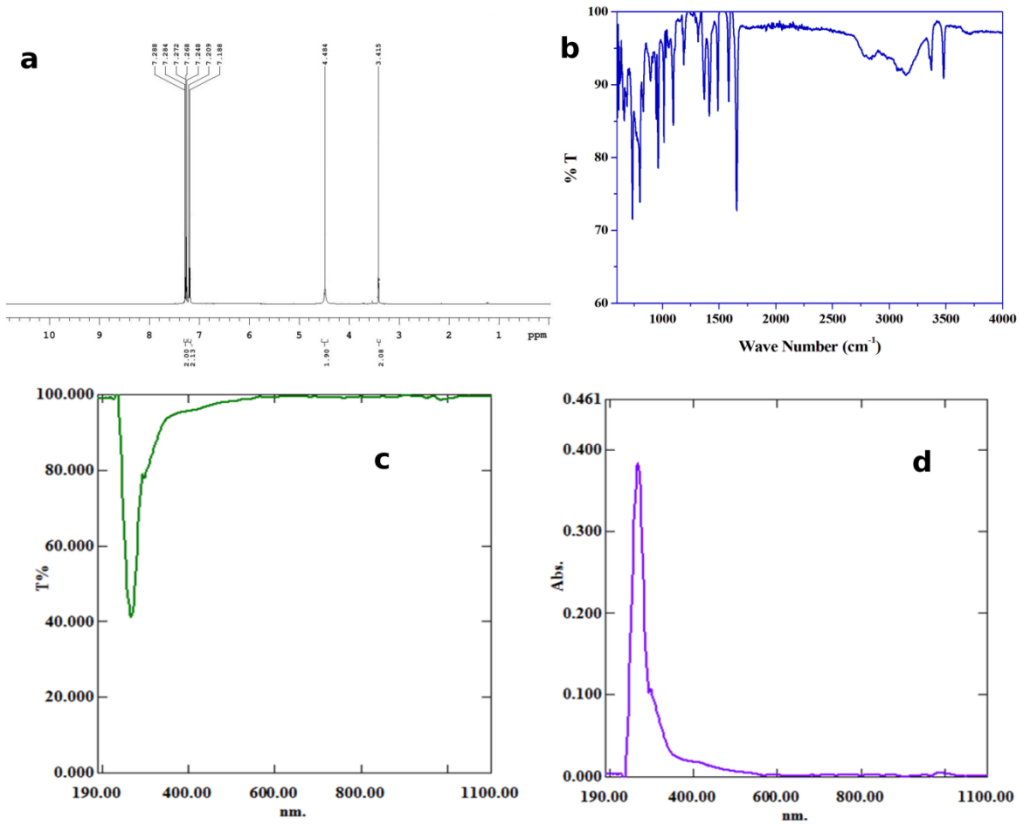

Figure 1. (a) 1H-NMR, **(b)** FT-IR, **(c)** and **(d)** UV-visible spectra of (Z)2-(4-chlorophenyl)-N'-hydroxyacetamidine.

3.3. Crystal structure and geometry optimization.

The structural analysis revealed that the (Z)2-(4-chlorophenyl)-N'-hydroxyacetamidine (CPHA) compound was crystallized in the monoclinic crystal system with the space group P21. The ORTEP of the molecule with thermal ellipsoids drawn at a 30% probability level is shown

in figure 2, and the crystallographic parameters are depicted in Table 1. The molecular structure of CPHA adopts a Z-conformation with respect to the C=N bond, and the double bond distance is 1.283(2), which confirms that it is in good agreement with the theoretical value. Torsional angles of 179.06° about O1-N2-C8-C7 and 1.21(3)°about O1-N2-C8-N1 confirm that the C7 atom and the amidoxime chain are planar. The chlorine-substituted phenyl ring, C1-C2-C3-C4-C5-C6, lies in the equatorial position with respect to the plane described by the amidoxime chain N1-C8-N2-O1 confirmed by the dihedral angle 82.74°. A torsion angle of 75.93 and -104.32 about N2-C8-C7-C4 and C4-C7-C8-N1 indicates antiplanar conformation and +synclinal conformation, respectively.

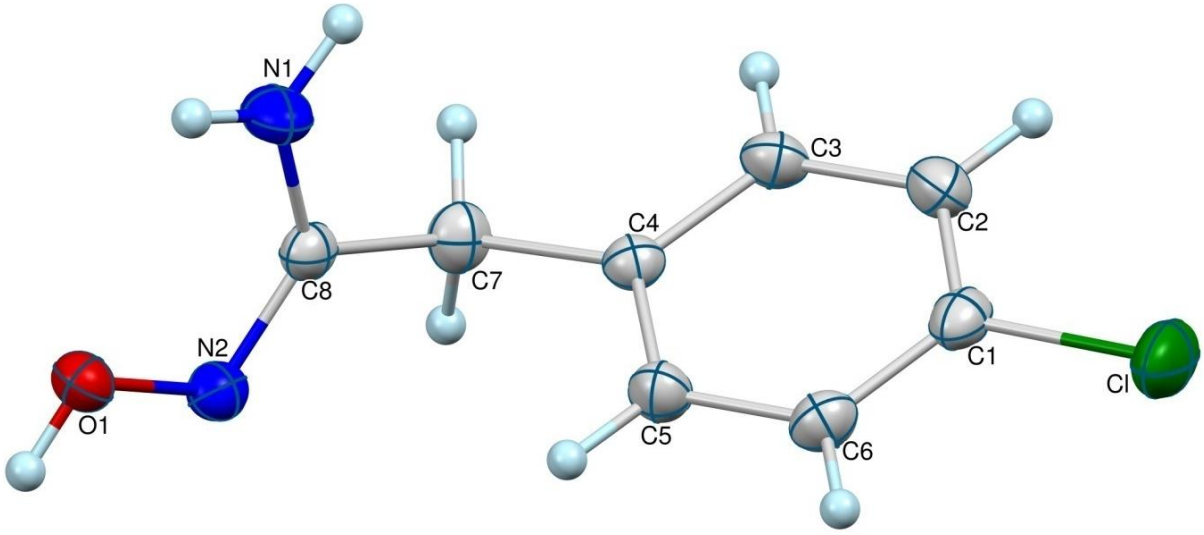

Figure 2. *ORTEP* of CPHA with the atomic numbering scheme.

The O1-N2 bond distance is 1.424(2), but due to intramolecular interaction, it is less than (1.446) the reported one [12]. The crystal structure of CPHA is stabilized by a number of intra and intermolecular interactions. Intramolecular N9–H9A…O11 interaction forms a five-membered planar ring C8/N1/H1A/O1/N2 with amidoxime chain (figure 3a) and also leads to the stretching of O-N bond by 0.022 Å (O1-N2: 1.424 Å) compared to standard amidoxime O-N bond distance 1.446 Å [13].

Hydroxyacetamidine group extensively involved in the formation N-H . . . O and O-H...N Intermolecular hydrogen bond interactions play a major role in molecular stability. NH_2 group formed two hydrogen bonds with hydroxyl oxygen, whereas O1 acts as both donor and acceptor by making O1-H1...N2 and N1-H1B...O1 interactions, respectively. These hydrogen bonds between NH2 and OH groups connect adjacent molecules to construct R22(7) and R44(11) synthons when viewed along the crystallographic a-axis (Figure 3b). The crystal structure of CPHA is also exhibiting C6-H6…π (C6–H6 . . . Cg1: C-Cg; 3.01 Å, C-H . . . Cg; 132° and with a symmetry code 1–x,1/2+y,1/2–z where Cg1 is the centroid of the chlorophenyl ring) and C-Cl...O intermolecular interactions, which are significant, contribute in the crystal structure stability (Figure 4).

Table 1. Crystal data and structure refinement details of CPHA.

Parameter	value
CCDC deposit No.	1490888
Empirical formula	C8H9ClN2O
Formula weight	184.62
Temperature	293 (2) K
Wavelength	0.71073 Å

Parameter	value
Crystal system, space group	Monoclinic, P21
Unit cell dimensions	a = 7.494 (10) Å b = 5.389 (8) Å c = 10.729 (15) Å α = 90o β = 91.350(6)o γ = 90o
Volume	433.24(11) Å3
Z	2
Density(calculated)	1.415 Mg m −3
Absorption coefficient	0.391 mm −1
F000	192
Crystal size	0.25 × 0.25 × 0.25 mm
θ range for data collection	3.28o to 27.46o
Index ranges	−9 ≤ h ≤ 9 −6 ≤ k ≤ 6 −11 ≤ l ≤ 13
Reflections collected	2484
Independent reflections	1071 [Rint = 0.0718]
Absorption correction	None
Refinement method	Full matrix least-squares on F2
Data / restraints / parameters	1071/ 1 / 109
Goodness-of-fit on F2	0.807
Final [I> 2σ(I)]	R1 = 0.0350, wR2 = 0.0973
R indices (all data)	R1 = 0.0364, wR2 = 0.0996
Extinction coefficient	0.04
Largest diff. peak and hole	0.250 and -0.188 e Å -3

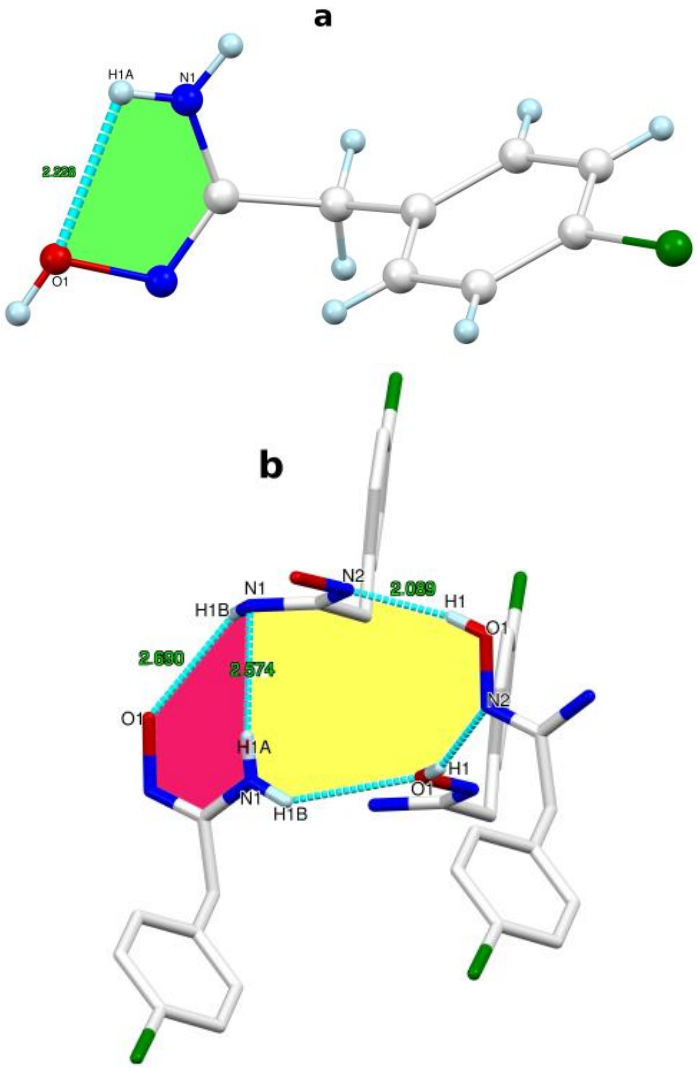

Figure 3. Supramolecular synthon of CPHA formed by intra and intermolecular hydrogen bond interactions.

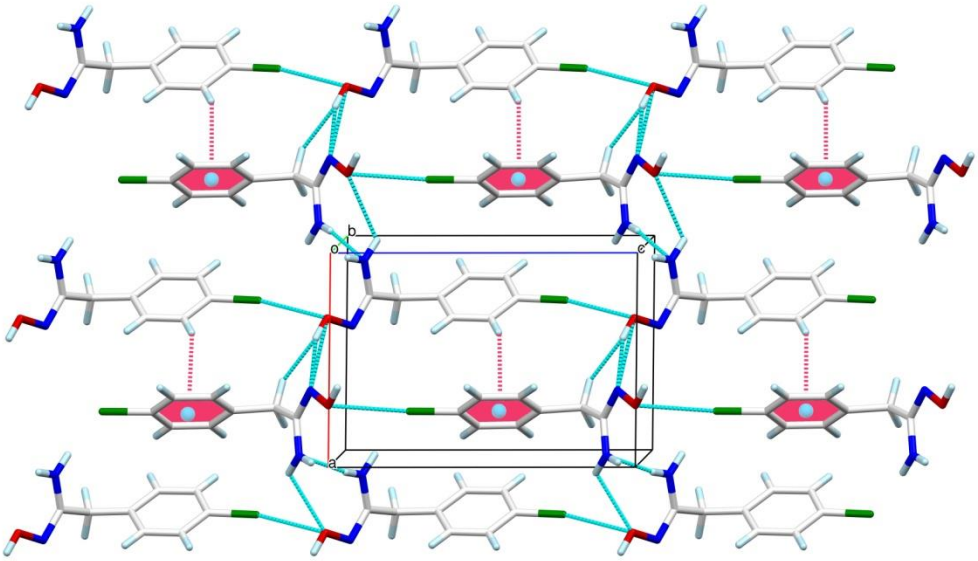

Figure 4. Crystal packing of CPHA viewed along *b*-axis**:** Intermolecular C-H...π, N-H...O, N-H...N, O-H...N, and C-Cl...O interactions are shown in dotted lines.

Table 2. Hydrogen bond geometry (Å, ◦).

D-H...A	D-H	H...A	D...A	D-H...A	Symmetry code
O(1)-H(1)...N(2)	0.82	2.09	2.8532	155	1-x, -1/2+y, -z
N(1)-H(1B) ...N(1)	O.86	2.57	3.4283	173	-x,-1/2+y,-z

Calculated frontier molecular orbitals (HOMO and LUMO) and selected bond parameters of CPHA are shown in figure 7 and tabulated in table 3. The HOMO of the CPHA is localized predominantly on the chlorophenyl group, whereas the LUMO is mainly localized on hydroxyacetamidine. Further, the values of energy gap (Eg = 2.89 eV), electronegativity (χ = 0.123 eV), absolute hardness (η = 0.052 eV), global softness (σ = 11.722 eV^{-1}), chemical potential (μ = -0.443 eV), and electrophile index (ω = 1.850eV) were calculated. The MEP map of the title compound gives a spectral view of raising potential value from red to blue. The potential value varies from $-2.673e^{-2}$ a.u. (deepest red) to $+2.673e^{-2}$ a.u. (deepest blue) for the title molecule. The blue regions are mainly localized on the hydrogen atoms of OH and NH groups of the title compound, presented in Figure 5.

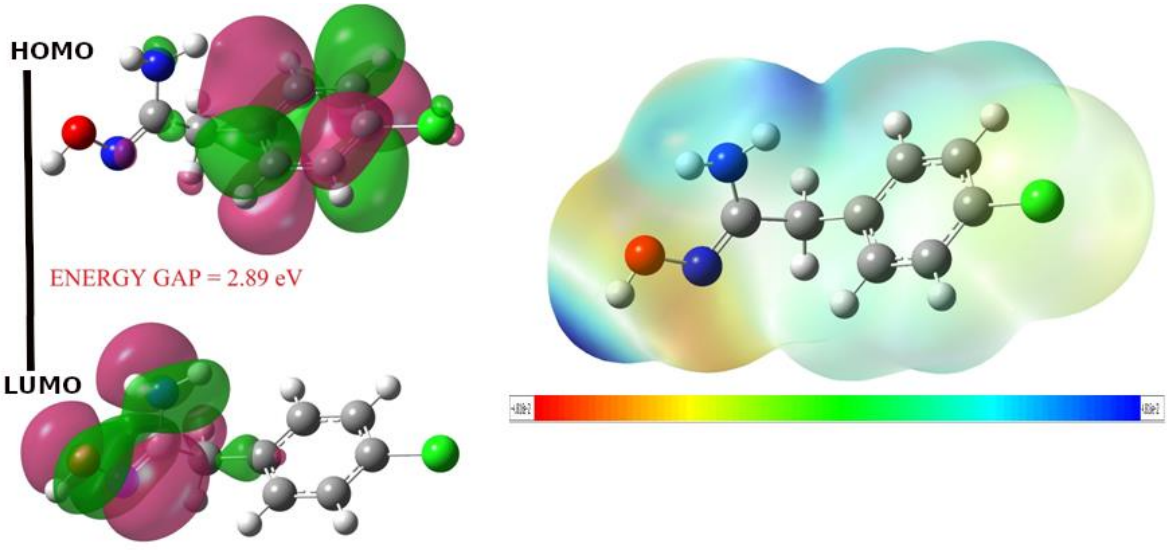

Figure 5. Frontier molecular orbitals (HOMO and LUMO) and molecular electrostatic potential of CPHA.

Table 3. Selected experimentally and theoretically determined bond lengths and bond angles of CPHA.

No.	Atom	Atom	Bond length (Å)		No.	Atom	Atom	Atom	Bond angles (°)	
			XRD	DFT					XRD	DFT
1	Cl	C1	1.740(2)	1.7593	1	Cl	C1	C2	120.0(2)	119.55
2	O1	N2	1.424(2)	1.4296	2	C2	C1	C6	121.3(2)	120.99
3	C1	C2	1.375(3)	1.3890	3	C1	C2	C3	118.7(2)	119.02
4	C1	C6	1.376(3)	1.3929	4	N2	C8	N1	124.2(2)	124.85
5	C2	C3	1.391(3)	1.3954	5	C7	C8	N1	117.8(2)	118.05
6	C8	N2	1.284(2)	1.2868	6	C3	C4	C5	117.9(2)	118.33
7	C8	C7	1.501(3)	1.5097	7	O1	N2	C8	110.0(1)	109.62
8	C8	N1	1.355(2)	1.3726	8	C1	C6	C5	119.4(2)	119.19
9	C4	C3	1.389(3)	1.3967	9	C2	C3	C4	121.6(2)	121.30
10	C4	C7	1.514(3)	1.5183	10	C8	C7	C4	113.4(2)	113.47
11	C4	C5	1.393(3)	1.4003	11	C4	C5	C6	121.1(2)	121.17
12	C6	C5	1.385(3)	1.3909	12	C7	C4	C5	120.0(2)	120.44
Correlation coefficient			0.9989		Correlation coefficient				0.9958	

3.3.1. Hirshfeld surface and energy frameworks analysis.

The Hirshfeld surface analysis comprising d_{norm} surfaces and 2D fingerprint plots were generated for the title compound in order to confirm the intermolecular interactions and to provide quantitative data for the relative contributions to the surfaces. d_{norm} surfaces of CPHA showed two dark red spots confirming the intermolecular O-H…N and N-H…O hydrogen bond interactions (Figure 6A). Fingerprint plots of the CPHA molecule suggest that the H…H interactions dominate the other interactions, with a 37.4 % contribution having a broad spike indicating the characteristic of the hydrogen bond. H…C, H…Cl, N…H and H…O forces also significantly contribute to the overall Hirshfeld surface (Figure 6B).

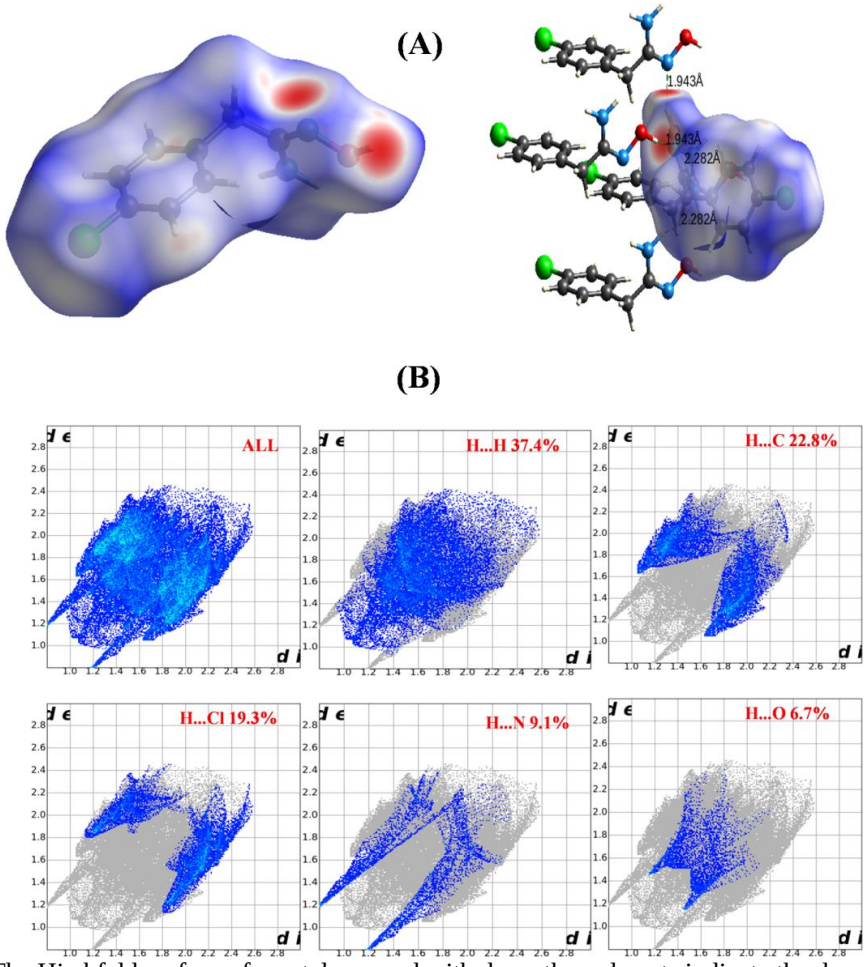

Figure 6. (A) The Hirshfeld surface of crystal mapped with d_{norm}, the red spots indicate the donor-acceptor sites and **(B)**. Fingerprint plots of the CPHA showing H...H, H...Cl, H...O, H...N and C...H interactions.

The interaction and lattice energy calculations were performed using the B3LYP/6-31 G(d,p) functional basis set. The electrostatic, polarization, dispersion, repulsion, and total interaction energies between the molecular pairs of radius 3.8Å were calculated and tabulated. The molecular pairs involved in the interaction are shown in Figure 7a. The molecular pair-wise interaction energies, electrostatic (E_{ele}=-73.25 kJ mol^{-1}), polarization (E_{pol}=-11.618 kJ mol^{-1}), dispersion (E_{dis}= -93.10 kJ mol- 15 1), repulsion (E_{rep}=71.99 kJ mol^{-1}) and the total interaction energy of the molecular pair is found to be -105.98 kJ mol^{-1} (table 4).

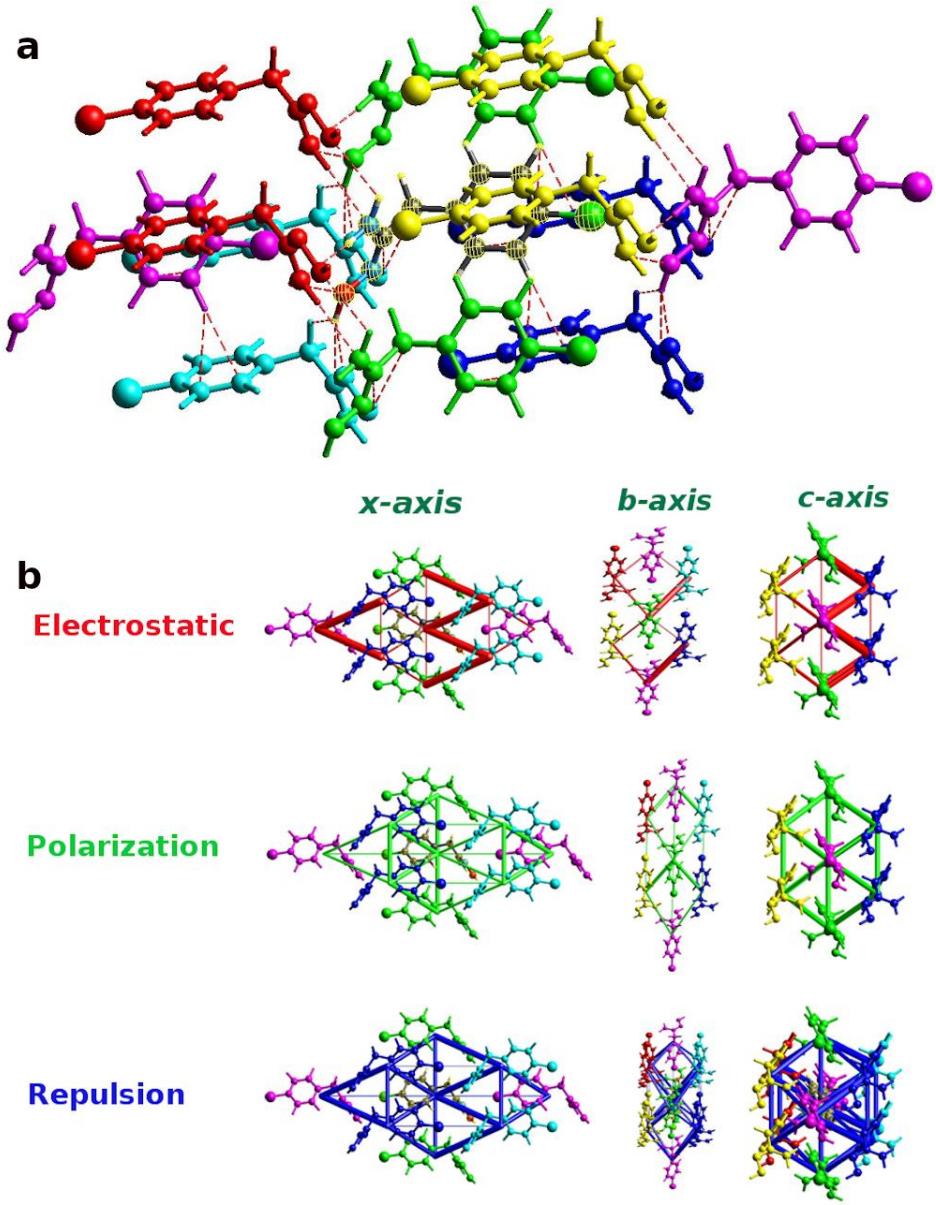

Figure 7. (a) Molecular pairs involved in the interaction energies calculation of CPHA and **(b)** the energy framework of the CPHA along *a*, *b*, and *c*-axes.

Table 4. Interaction energies (kJ/mol) of a pair of CPHA molecules (R: distance between centroids of molecules).

	N	Symop	R	E_ele	E_pol	E_dis	E_rep	E_tot
	2	-x, y+1/2, -z	8.91	-12.5	-2.1	-13.5	13	-18.6
	2	-x, y+1/2, -z	5.61	-8.9	-1.5	-25.2	17.4	-21.8
	2	x, y, z	5.39	-5.5	-1.2	-23.7	14.4	-18.4
	2	-x, y+1/2, -z	9.02	-37.1	-9.6	-12.4	46.9	-28.1
	2	-x, y+1/2, -z	5.45	-5	-0.9	-25.8	19.6	-16.3
	2	x, y, z	10.73	-0.3	-0.4	-6.3	5.2	-2.9

3.4. ADMET analysis.

For the assessment of the physicochemical and pharmacokinetics parameters throughout the drug development process, the ADMET (absorption, distribution, metabolism, excretion, and toxicity) for CPHA was determined, and the findings are explained. The compound demonstrated a high level of epidermal permeability and great gastrointestinal absorption. (log Kp > -2.5). The CPHA pretends as a P-glycoprotein substrate/inhibitor that demonstrated an excellent value of log VDss (I and II), as shown in Table 5. The blood-brain molecule easily crosses the CPHA barrier and enters the central nervous system. The possibility of the CPHA being a renel OCT2 substrate is low. One of the crucial and essential techniques in the realm of drug discovery is the prediction of toxicity. The pkCSM online tool was used to predict the toxicity of the CPHA molecule. The CPHA molecule's liver toxicity and skin sensitivity were investigated, with the findings presented in Table 5. Figure 8 shows a boiled egg and the bioavailability radar model of the CPHA.

Table 5. ADME and toxicity analysis of CPHA molecule.

	Parameters	Predicted value
Absorption	Water solubility (log mol/L)	-1.835
	Caco2 permeability (log Papp in 10^{-6} cm/s)	1.235
	Intestinal absorption (human) (% Absorbed)	89.893
	Skin Permeability (log Kp)	-2.289
	P-glycoprotein substrate	No
	P-glycoprotein I inhibitor	No
	P-glycoprotein II inhibitor	No
Distribution	VDss (human) (log L/kg)	-0.146
	Fraction unbound (human) (Fu)	0.423
	BBB permeability (log BB)	-0.064
	CNS permeability (log PS)	-2.279
Metabolism	CYP2D6 substrate	No
	CYP3A4 substrate	No
	CYP1A2 inhibitior	No
	CYP2C19 inhibitior	No
	CYP2C9 inhibitior	No
	CYP2D6 inhibitior	No
	CYP3A4 inhibitior	No
Excretion	Total Clearance (log ml/min/kg)	0.044
	Renal OCT2 substrate	No
Toxicity	AMES toxicity	Yes
	Max. tolerated dose (human) (log mg/kg/day)	0.723
	hERG I inhibitor	No
	hERG II inhibitor	No
	Oral Rat Acute Toxicity (LD50) (mol/kg)	2.366
	Oral Rat Chronic Toxicity (LOAEL) (log mg/kg_bw/day)	1.51
	Hepatotoxicity	No
	Skin Sensitisation	Yes
	T. Pyriformis toxicity (log ug/L)	0.084
	Minnow toxicity (log mM)	1.393

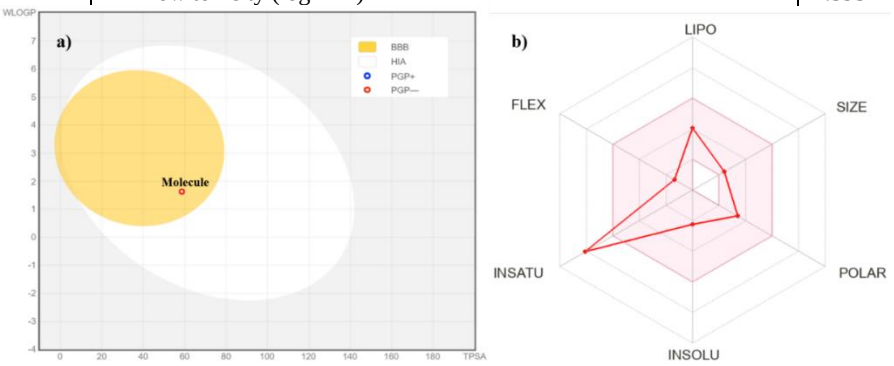

Figure 8. (a) Boiled egg and **(b)** bioavailability radar of CPHA molecule.

3.5. Swiss target prediction and STRING analysis.

SWISS software is a free web tool for the determination of the targets of synthesized analog. The synthesized compound was searched for targets in the Swiss Target Prediction database, which revealed related targets. The top 10 targets of each compound with probability > 0 were retrieved, and the duplicate targets were eliminated, resulting in a list of 100 targets in total. The obtained targets for CPHA were tabulated in Table 6. The compound shows a probability value of 0.125076 for all the targets, such as CA VII, I, III, VI, XII, XIV, XI, IV, VIII, and V. The CPHA molecule exhibits excellent probability values, as shown in Table 6. Results suggest CPHA is an excellent carbonic anhydrase inhibitor.

Table 6. Swiss predicted targets for CPHA molecule.

Target	Common name	Uniprot ID	Target Class	Probability*
Carbonic anhydrase VII	CA7	P43166	Lyase	0.125076
Carbonic anhydrase I	CA1	P00915	Lyase	0.125076
Carbonic anhydrase III	CA3	P07451	Lyase	0.125076
Carbonic anhydrase VI	CA6	P23280	Lyase	0.125076
Carbonic anhydrase XII	CA12	O43570	Lyase	0.125076
Carbonic anhydrase XIV	CA14	Q9ULX7	Lyase	0.125076
Carbonic anhydrase IX	CA9	Q16790	Lyase	0.125076
Carbonic anhydrase IV	CA4	P22748	Lyase	0.125076
Carbonic anhydrase XIII	CA13	Q8N1Q1	Lyase	0.125076
Carbonic anhydrase VB	CA5B	Q9Y2D0	Lyase	0.125076

3.6. Functional association of Carbonic anhydrase proteins.

Prediction of protein-protein relations was worked out among all identified protein species, and an interatomic network was obtained. From a functional perspective, an association can mean direct physical binding as well as indirect interactions. Figure 9 shows the PPI network for carbonic anhydrase (CA) proteins calculated by STRING. The STRING analysis showed a functional association of 6 proteins of CA (1AZM, 3CZV, 3ML5, 4YYT, 2HKF, and 4LU3) excluding 1ZNC protein. Among the best 7 hits, the protein 1ZNC was the best target and was the most closely (score: 0.721) associated with carbonic anhydrase IV protein, while 4YYT was the least (0.414).

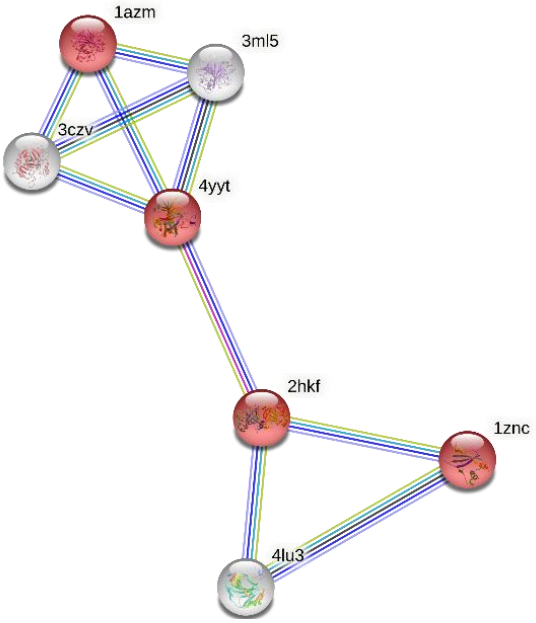

Figure 9. Protein-protein interaction analysis of carbonic anhydrase proteins using STRING.

3.7. Molecular docking studies.

Using *Auto dock vina* and *discovery studio* tools [27, 28], the molecular docking analysis of compound CPHA with 1ZNC protein was performed. It has been discovered that compound binding conformations are present in the active binding sites (Figure 10a). The interaction between the ligand and protein is shown in Figure 10b. CPHA molecule binds with ARG254, GLY252, VAL256, LYS37, ALA38, ILE33, LEU251, and VAL34 amino acid residues involving different types of interactions. The hydroxyacetamidine group of CPHA was active as a strong donor to form N-H . . . O and O-H...N hydrogen bonds with the ARG254 and GLY252 (C=O) residues (figure 10b and Table 7). The significant interactions between the CPHA molecule and targeted protein are also described by π-alkyl stacked interactions between centroids of the benzene ring and LYS37, LEU251, and VAL34 amino acid residues (figure 10b and table). Alkyl interactions between the chlorine atom of CPHA and ALA38, ILE33, and VAL256 residues are also explored in the binding site of the protein-ligand complex. Hence, it is clearly observed that CPHA molecule binds more favorably with 1ZNC protein.

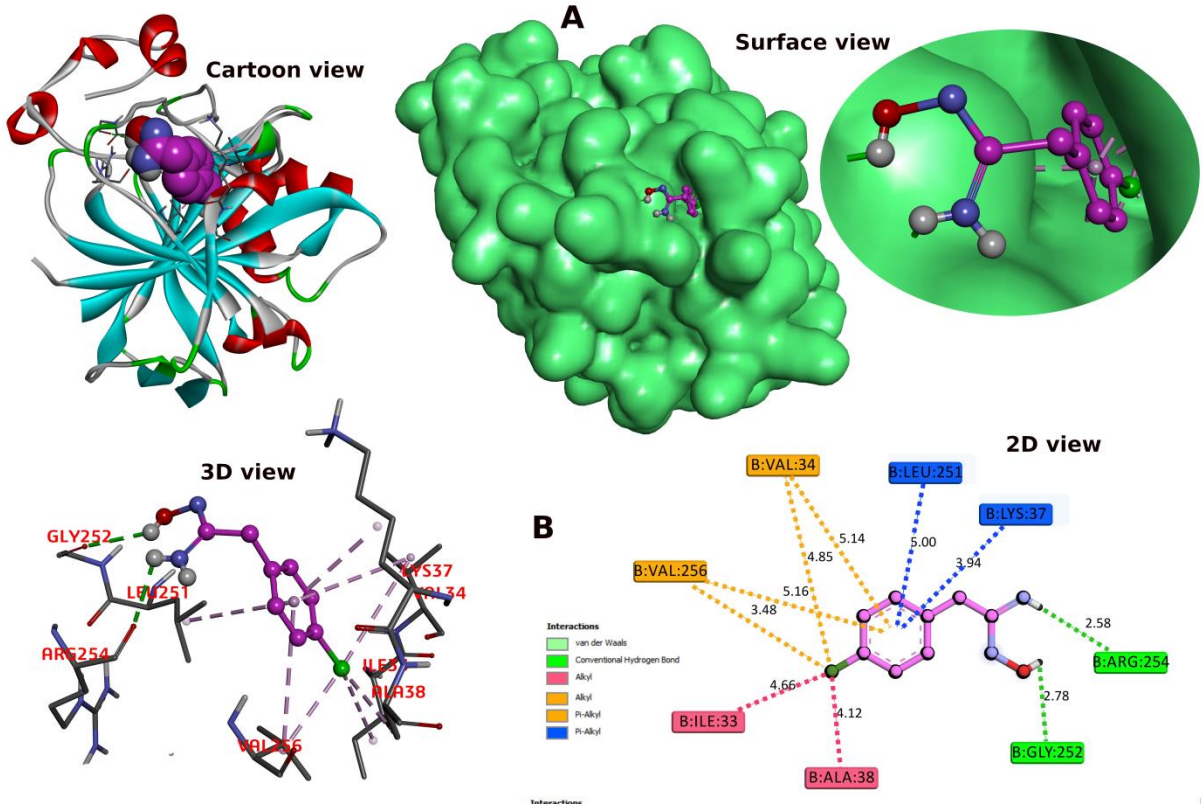

Figure 10. Molecular docking of CPHA with 1ZNC. **(A)** Docked poses with cartoon and surface representation **(B)** 3D and 2D view of CHPA-amino acid residues interactions in the active site of a protein.

Table 8. Interaction between ligand and 1ZNC protein.

Protein (amino acids)	Ligand	Interaction type	Distance (Å)	Binding score (kcal/mol)
ARG254	NH	conventional	2.58	-5.4
GLY252	OH	conventional	2.78	
VAL256	Chlorine	alkyl	3.48	
LYS37	Centroid of benzene	π-alkyl	3.94	
ILE33	Chlorine	alkyl	4.66	
ALA38	Chlorine	alkyl	4.12	
LEU251	Centroid of benzene	π-alkyl	5.00	
VAL256	Centroid of benzene	π-alkyl	5.16	
VAL34	Centroid of benzene	π-alkyl	5.14	

3.8. Molecular dynamic simulation.

For further examination of the molecular docking studies, the molecular dynamic simulation was performed. To investigate the binding mode stability and interactions between the targeted protein and the CHPA molecule, a simulation run spanning 100ns was carried out. The protein-ligand complex was analyzed by the root mean square deviation (RMSD), root mean square fluctuation (RMSF), and protein-ligand interactions to evaluate the dynamic characteristics over the simulation period (figure 11).

3.8.1. RMSD.

RMSD of the protein-ligand complex was examined during the 100ns MD simulation to measure the equilibration, protein flexibility, conformational changes, and translational and rotational movements inside the protein binding site. Figure 11A depicts the RMSD plot for the ligand-protein complex. CPHA molecule showed good stability, as this molecule is equilibrated at 0ns, vibrates about up to ~35ns, and then occurs stably between the span of ~3.5 Å during the entire simulation period. 1ZNC protein RMSD showed modest variation from 1 to 10 ns; subsequently, deviation stabilized consistently in the range between ~1.25 to 1.95 Å. During the simulation period, GLU123, ASN11, LYS43, and PRO85 residues showed a slight deviation of about 2.29, 1.96, 1.63, and 1.63 Å, respectively. The oscillations in the RMSD values for the CPHA-1ZNC complex indicated the durability of hydrogen and other bond interactions and showed that the CPHA molecule is more active inside the binding pocket of the 1ZNC protein.

3.8.2. RMSF.

RMSF for the protein-ligand complex was measured based on the fluctuations at the residue level. To explore more insight of the protein flexibility, the time average of RMSF values of all amino acids of 1ZNC protein with the presence of CPHA molecule were calculated over the simulation period. RMSF plot indicates that binding to the receptor was stable and showed a minor effect on the flexibility of the protein throughout the simulation period (figure 11B). The maximum fluctuation in the RMSF plot was observed for the residues GLU123 (2.29 Å), ASN11 (1.96 Å), LYS (1.63 Å), and PRO85 (1.63 Å). The active site residues LYS37, ILE33, ALA38, LEU251, ARG254, GLY252, and VAL256, which are contributed in the protein-ligand binding, showed less fluctuations of about 0.73, 0.44, 0.63, 0.69, 0.72, 0.97 and 0.47 Å respectively. In the RMSF plot, residues interacting with the ligand are spotted with green-colored vertical bars. ALA38 (0.063 Å), VAL40 (0.96 Å), GLY81(0.80 Å), GLY83 (0.97 Å), ASP139 (0.79 Å), GLU140 (0.79 Å), ALA142 (0.56 Å), ARG193 (0.39 Å), LEU195 (0.54 Å), VAL208 (0.49 Å), VAL256 (0.47 Å) and ILE257 (0.49Å) residues are interacted during simulation period with a less fluctuations.

3.8.3. Protein-ligand interactions.

Owing to their strong impact on drug specificity, metabolization, and adsorption, hydrogen bonds are very important in drug design. It is clear from the fingerprint image of the CHPA interaction at the protein active site the residues GLY83, ASP139, and GLU140 maintained their hydrogen bonds with the ligand during the simulation period (figure 11b). NH and NH_2 groups of CPHA sustained hydrogen bond interactions with ASP139, GLU140, and GLY83 with 84, 49, and 35% of the simulation time, respectively. ASP139 residue also forms

the ionic and water bridges with the OH group of CPHA. The residues VAL208 and LEU84 sustain their hydrophobic interactions (π-cation and π-π) with the aromatic groups of CHPA, which also significantly contribute to the overall protein-ligand stability during the simulation period.

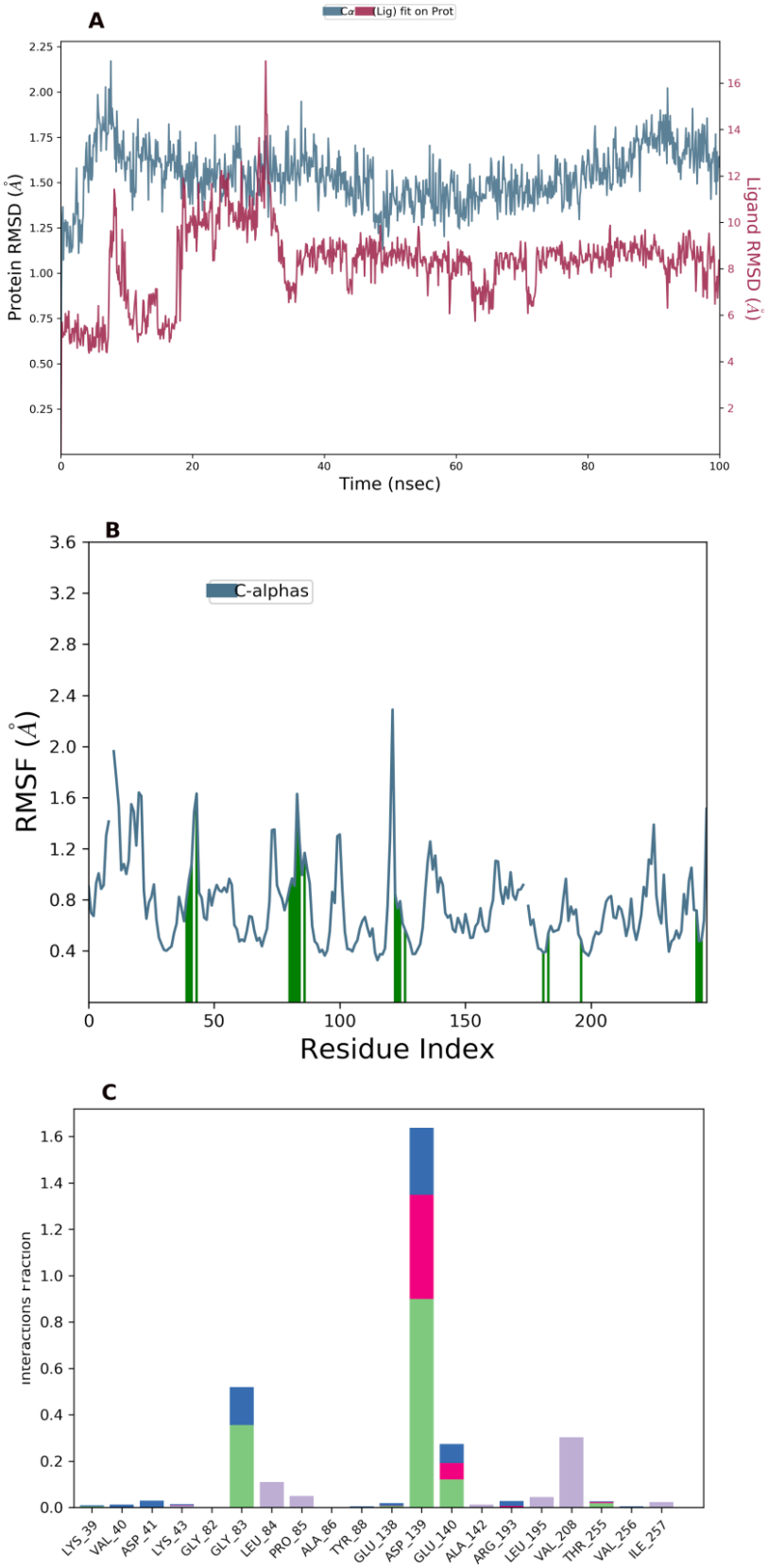

Figure 11. (A) RMSD, **(B)** RMSF profiles, and **(C)** fingerprints of protein-ligand interactions during the MD simulations.

4. Conclusions

(Z)-2-(4-chlorophenyl)-N'-hydroxyacetimidamide was synthesized and examined spectroscopically. Using a single crystal X-ray diffraction method, the 3D electrical structure was determined, revealing the molecular structure of (Z)-2-(4-chlorophenyl)-N'-hydroxyacetimidamide adopt Z-conformation with respect to the C=N. The structure displays both intra and intermolecular hydrogen bond interactions. Adjacent molecules are connected through O1-H1...N2 and N1-H1B...O1 interactions, which create R22(7) and R44(11) supramolecular synthons, responsible for the stability of the structure. All non-covalent intermolecular interactions were assessed via Hirshfeld surface analysis, revealing that H...H interactions (37.4%) significantly contribute to the total Hirshfeld surface. The investigation also examined the frontier molecular orbitals (HOMO and LUMO), determining an energy gap of 2.89 eV. The title compound revealed a low acute toxicity nature as well as a human maximum tolerated dose (0.723 log mg/Kg/day). SWISS target prediction suggested numerous targets for the CPHA molecule, and carbonic anhydrase IV with probability > 0 in the top 10 targets was chosen for the current study. A protein-protein interaction study has been performed to analyze the preferred target protein by String software. Molecular docking of the title compound with human carbonic anhydrase IV protein (PDB ID:1ZNC) is performed, and the binding affinity of -5.4 kcal/mol is obtained. The interactions between the ligand and the amino acid residues of the receptor are investigated by molecular dynamics (MD) simulation studies for 100 ns, and results revealed that the CPHA molecule is more stable inside the binding pocket of 1ZNC protein. In light of this, these *in-silico* features are notable. Furthermore, *in-vitro*, *in-vivo*, and clinical investigations are required to evaluate its potential.

Funding

This research received no external funding.

Acknowledgments

The authors would like to thank the National Facility Laboratory, the University of Mysore, Mysuru, for the instrumentation facility.

Conflicts of Interest

The authors declare no conflict of interest.

References

1. Fidan, I.; Salmas, R.E.; Arslan, M.; Şentürk, M.; Durdagi, S.; Ekinci, D.; Şentürk, E.; Coşgun, S.; Supuran, C.T. Carbonic anhydrase inhibitors: Design, synthesis, kinetic, docking and molecular dynamics analysis of novel glycine and phenylalanine sulfonamide derivatives. *Bioorganic & Medicinal Chemistry* **2015**, *23*, 7353-7358, https://doi.org/10.1016/j.bmc.2015.10.009.
2. Papastergiou, A.; Perontsis, S.; Gritzapis, P.; Koumbis, A. E.; Koffa, M.; Psomas, G.; Fylaktakidou, K. C. Evaluation of O-alkyl and aryl sulfonyl aromatic and heteroaromaticamidoximes as novel potent DNA photo-cleavers. *Photochem. Photobiol. Sci*., **2016,** *15*, 351-360. https://doi.org/10.1039/c5pp00439j
3. Ouattara, M.; Wein, S.; Denoyelle, S.; Ortial, S.; Durand, T.; Escale, R.;Vo-Hoang, Y. Design and synthesis of amidoxime derivatives for orally potent C-alkylamidine-based antimalarial agents. *Bioorg. Med. Chem. Lett.*,**2009,** *19*, 624-626. https://doi.org/10.1016/j.bmcl.2008.12.058

4. Bouhlel, A.; Curti, C.; Dumètre, A.; Laget, M.; Crozet, M. D.; Azas, N.; Vanelle, P. Synthesis and evaluation of original amidoximes as antileishmanial agents. *Bioorg. Med. Chem. Lett.*, **2010,** *18*, 7310-7320. https://doi.org/10.1016/j.bmc.2010.06.099
5. Nagahara, Y.; Nagahara, K. N-(2-Amino-5-chlorobenzoyl) benzamidoxime Derivatives Inhibit Human Leukemia Cell Growth. *Anticancer Res.*, **2014,** *34*, 6521-6526, https://pubmed.ncbi.nlm.nih.gov/25368254/.
6. Kayukova, L. A.; Praliev, K. D.; Akhelova, A. L.; Kemel'bekov, U. S.; Pichkhadze, G. M.; Mukhamedzhanova, G. S.; Nasyrova, S. R. Local anesthetic activity of new amidoxime derivatives. *Pharm. Chem. J.*,**2011,** *45*, 468-471. https://doi.org/10.1007/s11094-011-0657-0
7. Li, W.; Liu, R.; Kang, H.; Sun, Y.; Dong, F.; Huang, Y. Synthesis of amidoxime functionalized cellulose derivatives as a reducing agent and stabilizer for preparing gold nanoparticles. *Polym. Chem*.,**2013,** *4*, 2556-2563. https://doi.org/10.1039/C3PY00052D
8. Amidoximes: Promising Candidates for CO2 Capture Sonia Zulfiqara ,FerdiKaradas b , Joonho Park a , ErhanDeniz b , Galen D. Stucky c , Yousung Jung a , MertAtilhan b and Cafer T. Yavuz, Electronic Supplementary Material (ESI) for Energy & Environmental Science This journal is © The Royal Society of Chemistry 2011, https://pubs.rsc.org/en/content/articlelanding/2011/ee/c1ee02264d.
9. George A. P,; Paul R. R; Jack L. Synthesis and x-ray crystal structure of pyridine-2-amidoxime and aqua-bis-(pyridine-2-amidoxime) copper(II) chloride. *Polyhedron*, **1989,** *8*, 301-304. https://doi.org/10.1016/S0277-5387(00)80418-0
10. Kang, S. S.; Zeng, H. S.; Li, H. L.; Wang, H. B.; Wang, P. L. 4-Chlorobenzamidoxime. *ActaCrystallographica Section E: Structure Reports Online*, **2007,** *63*, o4698-o4698. https://doi.org/10.1107/S1600536807057273
11. Prabhuswamy, M.; Dinesha.; Pampa, K. J.; Kumar, S. M.; Nagaraja, G. K.; Lokanath, N. K. Synthesis, Crystal Structure and Characterization of (Z)-2-N′-hydroxyisonicotinamidine. Molecular Crystals and Liquid Crystals, **2014,** *593*, 243-252. https://doi.org/10.1080/15421406.2013.875735
12. Prabhuswamy, M.; Dinesha.; Abdoh, M. M. M.; Pampa, K. J.; Madan Kumar, S.; Nagaraja, G. K.; Lokanath, N. K. Synthesis, Crystal Structure, and Characterization of (Z)-2-(3-chlorophenyl)-N'-hydroxyacetamidine. *Mol. Cryst. Liq.*,**2015,** *606*, 189-198. https://doi.org/10.1080/15421406.2014.905087
13. Chahal, V.; Nirwan, S.; Pathak, M.; Kakkar, R. Identification of potent human carbonic anhydrase IX inhibitors: a combination of pharmacophore modeling, 3D-QSAR, virtual screening and molecular dynamics simulations. *J. Biomol. Struct. Dyn.*, **2022,** *40*, 4516-4531. https://doi.org/10.1080/07391102.2020.1860132
14. Türkeş, C.; Demir, Y.; Beydemir, Ş. Calcium channel blockers: molecular docking and inhibition studies on carbonic anhydrase I and II isoenzymes. *J. Biomol. Struct. Dyn* ,**2021,** *39*, 1672-1680. https://doi.org/10.1080/07391102.2020.1736631
15. Kumar, A.; Vashistha, V.K.; Das, D.K.; Ibraheem, S.; Yasin, G.; Iqbal, R.; Nguyen, T.A.; Gupta, R.K.; Islam, M.R. MNC-based single-atom catalysts for H2, O2 & CO2 electrocatalysis: activity descriptors, active sites identification, challenges and prospects. *Fuel*, **2021,** *304*, 121420. https://doi.org/10.1016/j.fuel.2021.121420
16. CrystalClear-SM Expert , Rigaku Corporation, Tokyo, Japan.**2011,** https://scripts.iucr.org/cgi-bin/paper?hb7428.
17. G. M. Sheldrick, *Acta Cryst.* Sec. A, **2008**, *64*, 112-122, https://www.scirp.org/(S(351jmbntvnsjt1aadkposzje))/reference/ReferencesPapers.aspx?ReferenceID=1217477.
18. A. L. Spek. *Acta Cryst.* Sec. A D Struct. Biol.,**2009,** *65(2)*, 148-155, https://doi.org/10.1107/s090744490804362x.
19. Mercury, Programme for crystal structure visualization and investigation of crystal structure (v 3.8). Cambridge crystallographic data centre, United Kingdom.**2017.**
20. Wang, A.; Kingsbury, R.; McDermott, M.; Horton, M.; Jain, A.; Ong, S.P.; Dwaraknath, S.; Persson, K.A. A framework for quantifying uncertainty in DFT energy corrections. *Sci. Rep.*,**2021,** *11*, 1-10. https://doi.org/10.1038/s41598-021-94550-5
21. Yang, H.; He, C.; Fu, L.; Huo, J.; Zhao, C.; Li, X.; Song, Y. Capture and separation of CO2 on BC3 nanosheets: A DFT study. Chinese Chemical Letters,**2021,** *32*, 3202-3206. https://doi.org/10.1016/j.cclet.2021.03.038
22. Spackman, P. R., Turner, M. J., McKinnon, J. J., Wolff, S. K., Grimwood, D. J., Jayatilaka, D. & Spackman, M. A. CrystalExplorer: a program for Hirshfeld surface analysis, visualization and qu-antitative analysis of molecular crystals, J. Appl. Cryst, **2021**, *54*, 3, 1006–1011 https://doi.org/10.1107/S1600576721002910

23. Sravika, N.; Priya, S.; Divya, N.; Jyotsna, P.M.S.; Anusha, P.; Kudumula, N.; Bai, S.A. Swiss ADME properties screening of the phytochemical compounds present in Bauhinia acuminata. *J. pharmacogn. phytochem.*,**2021,** *10*, 411-419. https://doi.org/10.22271/phyto.2021.v10.i4e.14193
24. Domínguez-Villa, F.X.; Durán-Iturbide, N.A.; Ávila-Zárraga, J.G. Synthesis, molecular docking, and in silico ADME/Tox profiling studies of new 1-aryl-5-(3-azidopropyl) indol-4-ones: Potential inhibitors of SARS CoV-2 main protease. *Bioorg. Chem.* **2021,** *106*, 104497. https://doi.org/10.1016/j.bioorg.2020.104497
25. Pair, F.S.; Yacoubian, T.A. 14-3-3 proteins: novel pharmacological targets in neurodegenerative diseases. *Trends Pharmacol. Sci.*, **2021,** *42*, 226-238. https://doi.org/10.1016/j.tips.2021.01.001
26. Dunkel, M.; Günther, S.; Ahmed, J.; Wittig, B.; Preissner, R. SuperPred: drug classification and target prediction. *Nucleic acids research*, **2008,** *36*, W55-W59. https://doi.org/10.1093/nar/gkn307
27. Gfeller, D.; Michielin, O.; Zoete, V. Shaping the interaction landscape of bioactive molecules. *J. Bioinform*, **2013,** *29*, 3073-3079. https://doi.org/10.1093/bioinformatics/btt540
28. Gong, J.; Cai, C.; Liu, X.; Ku, X.; Jiang, H.; Gao, D.; Li, H. ChemMapper: a versatile web server for exploring pharmacology and chemical structure association based on molecular 3D similarity method. *J. Bioinform*, **2013,** *29*, 1827-1829. https://doi.org/10.1093/bioinformatics/btt270
29. Gfeller, D., Michielin, O., & Zoete, V. Shaping the interaction landscape of bioactive molecules. *J. Bioinform*, **2013,** *29*, 3073-3079. https://doi.org/10.1093/bioinformatics/btt540
30. Daina, A.; Michielin, O.; Zoete, V. SwissTargetPrediction: updated data and new features for efficient prediction of protein targets of small molecules. *Nucleic Acids Res.*, **2019,** *47*, W357-W364. https://doi.org/10.1093/nar/gkz382
31. J. Eberhardt.; D. Santos-Martins.; A. F. Tillack.; S. Forli. AutoDock Vina 1.2.0: New Docking Methods, Expanded Force Field, and Python Bindings. *J. Chem. Inf. Model.***2021,** https://doi.org/10.1021/acs.jcim.1c00203
32. Eberhardt, J.; Santos-Martins, D.; Tillack, A.F.; Forli, S. AutoDock Vina 1.2. 0: New docking methods, expanded force field, and python bindings. Journal of Chemical Information and Modeling,**2021,** *61*, 3891-3898. https://doi.org/10.1021/acs.jcim.1c00203
33. Xu, L.Y., Alrefaei, Y., Wang, Y.S. and Dai, J.G., 2021. Recent advances in molecular dynamics simulation of the NASH geopolymer system: modeling, structural analysis, and dynamics. *Constr Build Mater*., **2021,** *276*, 122196. https://doi.org/10.1016/j.conbuildmat.2020.122196
34. Wang, E.; Fu, W.; Jiang, D.; Sun, H.; Wang, J.; Zhang, X.; Weng, G.; Liu, H.; Tao, P.; Hou, T. VAD-MM/GBSA: A Variable Atomic Dielectric MM/GBSA Model for Improved Accuracy in Protein–Ligand Binding Free Energy Calculations. *J. Chem. Inf. Model.*,**2021,** *61*,.2844-2856. https://doi.org/10.1021/acs.jcim.1c00091
35. Muzio, G.; O'Bray, L.; Borgwardt, K. Biological network analysis with deep learning. *Brief. Bioinform.*,**2021,** *22*, 1515-1530. https://doi.org/10.1093/bib/bbaa257
36. Moriarity, D.P.; Horn, S.R.; Kautz, M.M.; Haslbeck, J.M.; Alloy, L.B. How handling extreme C-reactive protein (CRP) values and regularization influences CRP and depression criteria associations in network analyses. *Brain Behav. Immun*., **2021,** *91*, 393-403. https://doi.org/10.1016/j.bbi.2020.10.020